Modeling the influence of etching defects on the sensitivity of MEMS convective accelerometers

A.A. Rekik[1,2], F. Azaïs[1], N. Dumas[1], F. Mailly[1], P. Nouet[1]
[1] LIRMM - CNRS/Univ. Montpellier 2 - 161 rue Ada, 34392 Montpellier, France
[2] ENIS - University of Sfax - Route Soukra, Cité Elhabib BP W 3052 Sfax, Tunisia

***Abstract*— In this paper, a behavioral model that includes the influence of etching defects on the sensitivity of MEMS convective accelerometers is presented. Starting from an existing behavioral model, new physically-based expressions have been derived to introduce etching defects in the simulation of thermal conduction in the sensor. In addition, a semi-empirical model has been introduced for thermal convection. Finally, a very good agreement is obtained between the behavioral model and FEM simulations.**

***Keywords*— MEMS, convective accelerometer, etching defects, fault modeling**

I. INTRODUCTION

In the field of Micro-Electro Mechanical Systems (MEMS) manufacturing, alternate test methods based on electrical test stimuli raise interest to facilitate testing and to reduce its cost [1]. Fault injection model can be used for evaluating test coverage [2] or for optimizing test stimuli [3]. In the case of mechanically actuated structures, high-level models allowing the injection of manufacturing defects are increasingly accurate for representative studies [4]. However, such models do not exist for convective sensors. Presently, evaluation of the influence of geometrical and material properties in convective accelerometers is only possible through Finite Element Modeling (FEM) [5,6], which is very time consuming and deals with a limited number of physical domains. The development of more compact models would ease the study of alternate test methods and more generally manufacturability issues.

In a previous study on MEMS convective accelerometers, we have shown that most of the parametric faults that affect the device specifications can be detected with electrical test measurements [5]. In particular, easily detected faults concern variations of both electrical and thermal resistances, and lateral geometrical parameters. Faults that escape to electrical tests are related to the convective behavior of the device. However, the correlations that may exist between the conductive and convective parameters were not taken into account in the model used for fault injection. In addition, the influence of the cavity depth was not included in this model, although it has been shown that this parameter significantly affects the device sensitivity [8]. It is therefore the objective of this paper to develop a high-level behavioral model to inject faults related to the cavity depth and to represent the potential correlations between conductive and convective phenomenon.

In this paper, we first briefly describe the accelerometer together with its previously published high-level behavioral model. In the second part, we detail the model development considering the main blocks of the model (heater source, fluid conduction, fluid convection and transduction). Finally, in the last part, we validate this new semi-empirical model with FEM simulations for different set of parameters and we illustrate benefits of such a model for alternate testing of MEMS convective sensors.

II. DEVICE UNDER TEST

A. Device Description

The device under test is a convective accelerometer obtained by Front-Side Bulk Micromachining (FSBM) of a CMOS die fabricated in a 0.8 µm technology from Austria Microsystems® (Fig.1). Main lateral dimensions are the half-width of both the heater beam (r_1) and the cavity (r_2), and the distance between the heater and one detector (d). The three thin bridges are composed of the CMOS process back-end layers (oxide, polysilicon, aluminum, and nitride). In particular, polysilicon is used to implement resistors, for both heating (R_H) and temperature sensing (R_{D1}, R_{D2}). The heater R_H is powered with an electrical voltage (U_H) to create a temperature gradient in the bottom (i.e. etched silicon) and top (i.e. package) cavities: the temperature is then maximum at the heater location and minimum at the cavities boundaries.

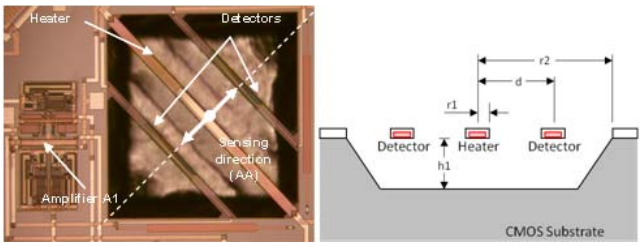

Figure 1. SEM picture of the prototype and geometrical parameters: r_1=20µm, r_2=350µm, d=175µm, h_1=390µm

In absence of acceleration, the temperature detectors (R_{D1}, R_{D2}) are located on identical temperature gradients for symmetry reasons. Under acceleration along the AA'-axis, the cavity temperature distribution deforms due to free convection and detectors may measure the differential temperature. Indeed, polysilicon resistivity exhibit high temperature dependence (Temperature Coefficient of Resistance, TCR=9×10^{-4}/°C) and the thermal signal is easily converted into a voltage by means of a Wheatstone bridge. This voltage is then amplified by an instrumentation amplifier. For more details on sensor

978-1-4244-7791-3/10/$26.00 ©2010 IEEE

manufacturing and characterization, please refer to previous works from some of the authors [6,9].

B. Device model

For system-level and electronic interface circuit design, a behavioral model of the sensor was developed and implemented in both Matlab/Simulink® and Cadence® [10]. This model (Fig.2) is composed of four main blocks. First, the heater temperature (T_H) is calculated from the external power supply (U_H). Then, regarding fluid conduction, an analytical expression based on solving the heat conduction in a cylindrical geometry approximation is used to compute the common mode temperature (T_{CM}) of the detectors. This expression involves lateral sensor dimensions (r_1, r_2 and d). Regarding fluid convection, the differential temperature (ΔT_D) resulting from an acceleration is calculated with an empirical expression that involves fitting parameters. Finally, regarding transduction, both detector resistances (R_{Di}) are deduced from their *TCR*. This model was calibrated with silicon data and FEM simulation.

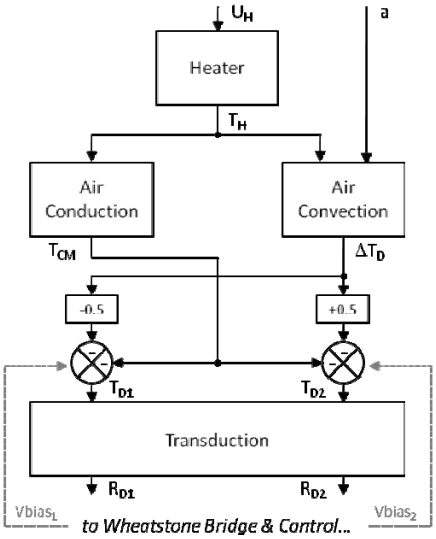

Figure 2. Block diagram of the sensor model

C. Manufacturing defects and fault modeling

Process scattering will affect some model parameters. For instance, the nominal value of the electrical resistances depends on polysilicon doping, thickness, width and length (a typical 3σ dispersion of about 20% is usually considered). In the same way, the resistance temperature coefficient *TCR* will be affected by doping concentrations. All these variations are global variations that affect every block of the model in the same way. In addition, process scattering will also introduces local variations that should be modeled as mismatch errors.

Regarding lateral dimensions, these are parameters that are rather well-controlled in the manufacturing process. They are nevertheless subject to variations, but with a low dispersion. Note that the distance d between the heater and the detector bridge is set by the mask and therefore should not change from one fabricated device to another.

Note that contrary to lateral dimensions, the cavity depth is a parameter that is very difficult to control. Indeed, it is very sensitive to the etching process (etching solution composition, etching time and etching solution movements). As the optical control is not an easy task during etching, the cavity depth is likely to be reduced if ideal conditions are not met during the etching step.

III. BEHAVIORAL MODELING

This section details the development of the behavioral model that includes the influence of the cavity depth, considering the 4 main blocks of the initial model, i.e. the heater source, fluid conduction, fluid convection and transduction.

A. Heater source

During normal operation, the heating bridge is powered with a dc voltage (U_H) in order to set an initial temperature distribution in the cavity. The average heater temperature (T_H) is directly linked to the electrical power (P_H) with a linear relationship:

$$T_H = T_A + Rth_H \cdot P_H = T_A + Rth_H \cdot \frac{U_H^{\,2}}{R_H} \tag{1}$$

where T_A is the ambient temperature, R_H is the electrical resistance of the beam and Rth_H is the thermal resistance of the heater beam.

The temperature dependence of the electrical resistance is taken into account in the power dissipation with:

$$R_H = R_{H0}\left(1 + TCR \cdot \Delta T_H\right) \tag{2}$$

where *TCR* is the temperature coefficient given by the foundry and R_{H0} is the nominal value of the heater resistance at a reference temperature T_0. This electrical resistance is obviously independent of the cavity depth but just depends on the size of the heating resistance and on the material properties.

In contrast, the thermal resistance of the beam depends not only on the beam dimension but also on its geometrical environment. In order to evaluate the influence of the cavity depth on this parameter, we have performed a number of FEM simulations for different values of the cavity depth between 35µm and 490µm and different values of the heater temperature from 350K to 600K, and we have recorded the heat transfer coefficient h_H (in $W.m^{-2}.K^{-1}$). This coefficient writes:

$$h_H = \frac{1}{Rth_H \cdot S} \tag{3}$$

where $S = 54.7 \times 10^3$ µm² is the exchange surface between the beam and the fluid given by $2(2r_1+e)L$, with L the beam length and e the beam thickness.

Figure 3 reports the heat transfer coefficient (h_H) with respect to the cavity depth h_1 for different heater temperatures T_H. The higher the heater temperature is, the higher the heat

transfer coefficient. This phenomenon is only due to the variation of air thermal conductivity which increases with temperature.

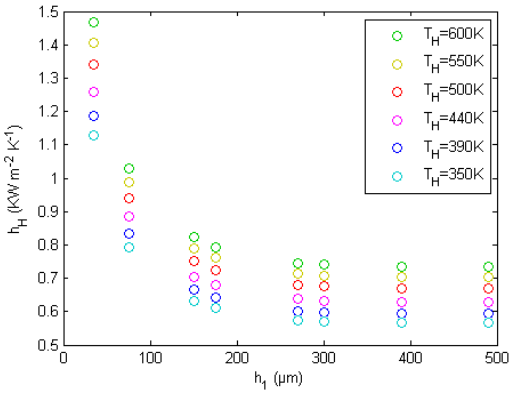

Figure 3. Heat transfer coefficient vs. cavity depth for different heater temperatures

This dependence must be included in the model in order to enable the simulation of the device under different biasing conditions. Two behaviors can be distinguished:

- for high values of the cavity depth, the heat transfer coefficient is constant,
- for low values of the cavity depth, the heat transfer coefficient increases when the cavity depth decreases.

This can be explained by the shape of the hot bubble created by the heater, as illustrated in figure 4. When the cavity depth is high enough, the lateral silicon walls of the cavity limit the size of the hot bubble. The size of this hot bubble is therefore not affected by the value of the cavity depth and the heat transfer coefficient just depends on the heater temperature and lateral dimensions. In contrast, for low values of the cavity depth, this parameter becomes the limiting factor and the size of the hot bubble tends to reduce. In this case, the heat transfer coefficient depends on the heater temperature, the heater width and the distance between the heater and the bottom of the cavity. The transition between these two behaviors occurs around h_1=175µm, which corresponds to half the distance between the heater and the lateral cavity border (r_2). Note that this threshold does not depend on the heater temperature.

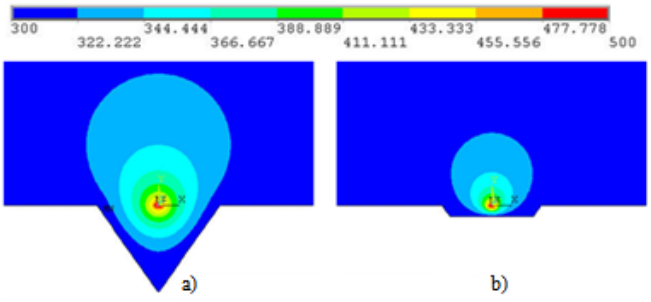

Figure 4. Temperature profile within cavity for two different values of the cavity depth – a) h_1=490µm and b) h_1=75µm

From this analysis, we have derived an analytical model for the heat transfer coefficient. This model relies on the assumption that we have a radial heat flow in a cylindrical geometry. Considering the expression of air conductivity from 100K to 600K: $\lambda(T)=\lambda_0\cdot\left(1+\delta_1 T+\delta_2 T^2+\delta_3 T^3\right)$ with λ_0 the air conductivity extrapolated at 0K, and δ_1, δ_2 and δ_3 the coefficients of thermal variation of conductivity for air.

Integrating the Fourier law for heat conduction $\Phi=-\lambda_{air}\,\mathrm{grad}(T)$ in a cylindrical geometry, we can express:

$$h_H=\frac{\lambda_0}{R_1\cdot ln\left(\frac{R_2}{R_1}\right)}\cdot\left(1+\frac{\delta_1}{2}\cdot\frac{T_H{}^2-T_A{}^2}{T_H-T_A}+\frac{\delta_2}{3}\cdot\frac{T_H{}^3-T_A{}^3}{T_H-T_A}+\frac{\delta_3}{4}\cdot\frac{T_H{}^4-T_A{}^4}{T_H-T_A}\right) \quad (4)$$

where R_1 and R_2 correspond to the radius of the cylinders representing the heater and the hot bubble respectively.

Note that this equation includes the dependence with respect to the heater temperature T_H. To include the dependence with respect to the cavity depth, we have then established the radius of the equivalent cylinder R_2=f(h_1), which would give the heat transfer coefficient obtained by FEM simulations (Figure 5). First, we have determined the different values of h_H for different values of the etching cavity (h_1). Second, we have calculated the cylinder equivalent radius R_2 to minimize the error using equation (4) to represent the values of h_H previously determined for each value of h_1. In that step, we consider a cylinder equivalent radius R_1=16µm for the heater. This value is a trade-off between a cylinder with a perimeter equivalent to the heater bridge perimeter and a cylinder that contains the heater beam.

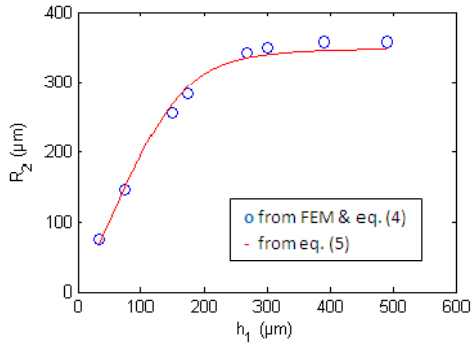

Figure 5. Size of the equivalent cylinder representing the hot bubble vs. cavity depth

Finally, we express the equivalent radius of the hot bubble R_2 to reflect a linear relationship for low values of h_1 and a saturation at r_2=350µm for high values of h_1 with a transition at r_2/2:

$$R_2=r_2\cdot\frac{h_1}{\sqrt[4]{h_1{}^4+\left(\frac{r_2}{2}\right)^4}} \quad (5)$$

The order of the denominator polynomial has been chosen for adequate transition between both regions (Figure 5).

B. *Fluid conduction*

The initial temperature of both detectors, i.e. the common mode temperature T_{CM}, is also controlled by heat conduction in

the air. The same assumption of a radial heat flow in a cylindrical geometry can therefore be used. The relationship between the common mode temperature T_{CM} and the heater temperature T_H can then be obtained by solving heat conduction equation at a distance d from the heater:

$$(T_{CM}-T_A)+\frac{\delta_1}{2}\left(T_{CM}{}^2-T_A{}^2\right)+\frac{\delta_2}{3}\left(T_{CM}{}^3-T_A{}^3\right)+\frac{\delta_3}{4}\left(T_{CM}{}^4-T_A{}^4\right)= \frac{\ln\left(\frac{d}{R_2}\right)}{\ln\left(\frac{R_1}{R_2}\right)}\cdot\left((T_H-T_A)+\frac{\delta_1}{2}\left(T_H{}^2-T_A{}^2\right)+\frac{\delta_2}{3}\left(T_H{}^3-T_A{}^3\right)+\frac{\delta_3}{4}\left(T_H{}^4-T_A{}^4\right)\right) \quad (6)$$

In the same way than in the previous section, we have determined the size of the equivalent cylinder R_2' that gives the best fit between the common mode temperatures T_{CM} calculated with equation (6) and measured in FEM simulations. Results are summarized in figure 6 for various cavity depth h_1.

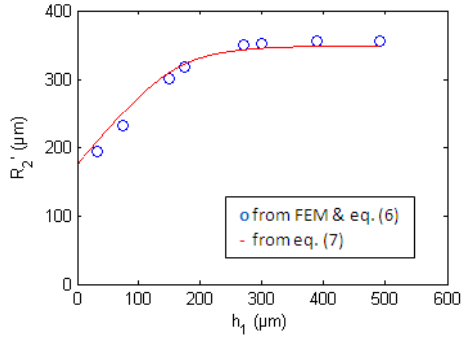

Figure 6. Size of the equivalent cylinder governs the common mode temperature vs. cavity depth

Similarly, we observe a linear relationship for low values of h_1 and a saturation at r_2=350µm for high values of h_1, with a transition at $r_2/2$. However, in the linear region, the reduction of the size of the equivalent cylinder is less important than in the previous case. This is due to the fact that the common mode temperature is measured on a specific axis (i.e. sensitive axis) whereas the total heat flow is an average effect along all the directions and is dominated by the smaller distance.

As a result we have to consider, for the determination of the common mode temperature T_{CM}, an equivalent cylinder with a radius R_2' different than the one used for the determination of the heat transfer coefficient. The relationship between this radius and the cavity depth can be analytically expressed by:

$$R_2'=(r_2-d)\cdot\frac{h_1}{\sqrt[4]{h_1{}^4+\left(\frac{r_2}{2}\right)^4}}+d \quad (7)$$

As illustrated in fig. 6, there is a good agreement between this expression and values established using FEM simulations.

C. Fluid convection

The sensor sensitivity is proportional to the differential temperature between both detectors in presence of acceleration along the sensitive axis. This temperature variation is due to free convection and can be analytically solved only for very simple geometries. For complex geometries FEM simulations are mandatory to calculate the differential temperature.

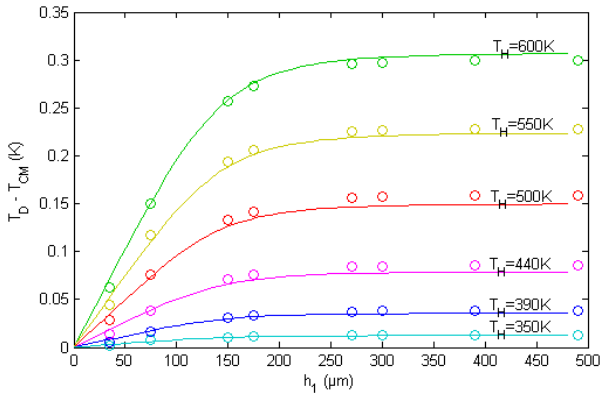

Figure 7. Differential temperature ($\Delta T_D/2$) vs. cavity depth for different heater temperatures (solid line: model, dots: FEM)

Figure 7 shows the differential temperature T_D-T_{CM} =$\Delta T_D/2$ according to the cavity depth h_1 and to the heater temperature T_H. Results are given for an acceleration of 1g along the sensitive axis and for the nominal distance d=175µm. As for the heat transfer coefficient and for the same reasons, the differential temperature ($\Delta T_D/2$) saturates for high values of h_1. For small depths, the differential temperature is proportional to h_1 and the transition between the two regions occurs around h_1=150µm. For a given depth, the differential temperature is proportional to $(T_H$-$T_A)^{1.8}$. Equation 8 gives the semi-empirical expression established to represent this behavior, which involves some fitting parameters and sensor dimensions:

$$T_D-T_{CM}=10.84\times10^{-6}\cdot\frac{h_1}{\sqrt[4]{h_1{}^4+\left(150\cdot10^{-6}\right)^4}}\cdot\frac{4(d-r_1)(d-r_2)}{(r_1-r_2)(r_2-r_1)}\cdot(T_H-T_A)^{1.8}*a \quad (8)$$

where 10.84×10^{-6} $K^{-1.8}$/g is a constant linked to the thermo-physical properties of air and to the height of the top cavity (10mm for these simulations).

Figure 7 shows a good agreement between this expression and FEM simulations, with a relative error that remains below 6%.

D. Transduction

The role of the detectors is to convert thermal signal variations into electrical resistance variations thanks to the temperature sensitivity of polysilicon. Using a Wheatstone bridge, these resistance variations can then be translated into voltage variations for further conditioning. The electrical resistance of each detector R_{Di} is simply given by:

$$R_{Di}=R_{Di_0}\left(1+TCR\cdot\left(T_{CM}-T_0\pm\frac{1}{2}\Delta T_D+Rth_D\cdot\frac{Vbias_i{}^2}{R_{Di_0}}\right)\right) \quad (9)$$

where R_{Di0} is the nominal value of each detector resistance at reference temperature T_0. , and V_{biasi} is the biasing voltage of each detector.

Note that this expression includes self-heating of the detectors, and therefore involves the thermal resistance of the detectors. This thermal resistance Rth_D depends on the cavity depth as it is influenced by the geometrical environment. However because the detectors have a high resistance value of 50kΩ, the self-heating impact is almost negligible. Consequently, we have not modeled the dependence of the cavity depth on the detector thermal resistance.

IV. VALIDATION & EXPLOITATION

A. Model validation

Model validation with respect to FEM simulations is based on numerous experiments for different values of the etching cavity depth. First, we have compared the calculated heater thermal resistance with the value determined from FEM simulations. Results are summarized in figure 8.a. It can be seen that we have a very good agreement whatever the heater temperature, with a relative error that remains below 2%.

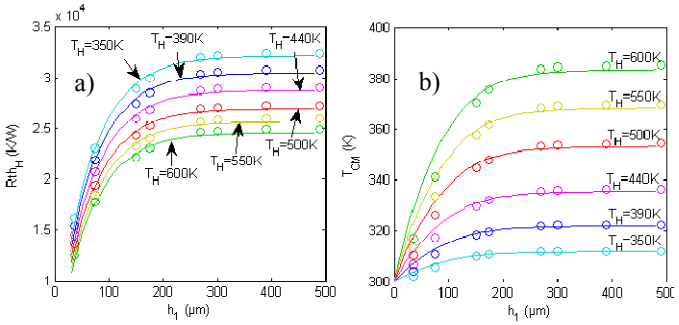

Figure 8. Comparison between behavioral model and FEM simulation for the heater thermal resistance Rth_H (a) and for the common mode temperature T_{CM} (b) (solid line: model, dots: FEM)

Then, we have calculated the detectors' common mode temperature and we have reported these values together with results from FEM simulations (Fig.8.b). Here again a good agreement is observed whatever the heater temperature and h_1 are, with a relative error that remains below 4%.

B. Model exploitation

Interestingly, the common mode temperature (Fig.8.b) and the differential temperature (Fig.7) present very similar behaviors. As an illustration, figure 9 plots the differential temperature $\Delta T_D/2$ resulting from a 1g acceleration vs. the common mode temperature T_{CM}, measured in FEM simulations on devices with different cavity depths ranging from 35µm up to 490µm. It clearly appears that, for a given heater temperature, both temperatures are strongly correlated. This is very interesting because the differential temperature ΔT_D results from the application of acceleration and therefore directly relates to the device sensitivity, while the common mode temperature T_{CM} just depends on the biasing conditions of the structure. In other words, it means that etching defects that affect the device sensitivity also affect the detectors' common mode temperature in a similar way. Hence, verifying the common mode temperature in absence of acceleration may be a way to verify the device sensitivity to a given acceleration. However, it should be underlined that this result is obtained for a fixed heater temperature, and for a device with all parameters at nominal value except the cavity depth that varies from 35µm to 490µm. Practically, the heater temperature T_H cannot be imposed but only the biasing voltage of the heater beam U_H, and the device parameters obviously exhibit some dispersions.

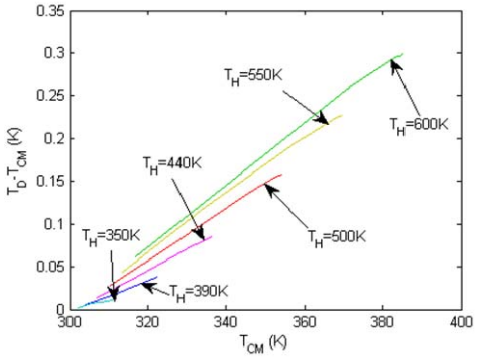

Figure 9. FEM simulation results: differential temperature ($\Delta T_D/2$) due to a 1g acceleration vs. common mode temperature

To further explore this possibility, the behavioral model that includes the influence of the cavity depth can be very helpful. Indeed it is not realistic to perform Monte-Carlo FEM simulations, but on the contrary the behavioral model easily supports Monte-Carlo simulations at system-level. In this objective, we have performed experiments considering the following dispersions on the parameters' model:

- A Gaussian variation with a standard deviation of 3σ=20% on the value of the electrical resistances. This variation corresponds to the typical uncertainty given by the foundry and is a global variation, i.e. it affects all resistances in the same amount.
- A Gaussian variation with a standard deviation of 3σ=2µm on the value of the geometrical parameters related to horizontal dimensions, i.e. the heater dimension r_1 and the distance r_2 between the heater and the border of the cavity. Indeed lateral dimensions are parameters that are rather well-controlled in the manufacturing process and therefore exhibit a low dispersion. Note that the distance d between the heater and the detectors is not subject to process variations due to mask self-alignment.
- A Gaussian variation with a standard deviation of 3σ=10% on TCR has been set as it is well-known that this parameter is quite sensitive to doping fluctuations.
- A uniform variation on the value of the cavity depth h_1 between 35µm and 490µm, since it is the objective to investigate the influence of this parameter.

Potential asymmetries have also been introduced in the model. In particular, a mismatch error with a standard deviation of 3σ=2% has been considered for the nominal value of the electrical resistance of the detectors R_{Di0} and the value of the reference resistors R_{REFi}.

Simulations have been performed on 1,000 runs and we have first observed the dispersion on the heater temperature (Fig.10.a) for a fixed biasing voltage U_H=2V of the heater resistance. It clearly appears that the influence of the cavity depth on the heater thermal resistance has a significant impact on the achieved heater temperature. By taking into account this dispersion, the proposed model hence permits to achieve realistic fast system-level simulations, which would be extremely time-consuming in FEM since it requires 3D simulations involving both solid and fluidic elements.

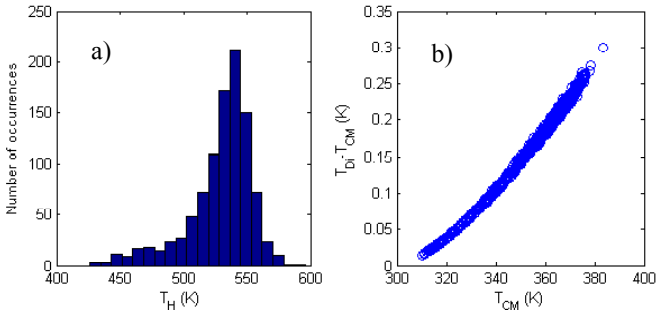

Figure 10. Behavioral model Monte-Carlo simulation results: dispersion on the heater temperature with U_H=2V (a) and differential temperature (ΔT_D/2) due to a 1g acceleration vs. common mode temperature (b)

Figure 10.b gives the differential temperature ΔT_D/2 resulting from a 1g acceleration vs. the common mode temperature T_{CM}, for a biasing of the heater beam at 2V. These results confirm that, even in presence of process variations, a rather good correlation exists between both temperatures. It is worth noting that the nominal value of the cavity depth is h_1=390µm, which corresponds to an average heater temperature of about 540K when the heater beam is biased at 2V, which in turns translates into a common mode temperature in the range of 360K to 380K. In this region, we can observe a linear relationship between the common mode temperature T_{CM} and the differential temperature ΔT_D/2.

More generally, the correlation that exists between the common mode temperature T_{CM} and the differential temperature ΔT_D offers an attractive perspective towards a low-cost test solution to verify the device sensitivity without the need for applying a calibrated acceleration. Indeed, the detectors' common mode temperature does not depend on the acceleration and is therefore a parameter that may be evaluated using only an electrical test setup.

V. CONCLUSION

In this paper, we have developed a behavioral model that includes the influence of etching defects on the sensitivity of MEMS convective accelerometers. Indeed, if lateral dimensions are rather well-controlled during the manufacturing process, this is not the case for the cavity depth which is very sensitive to the etching process conditions. Moreover, this parameter influences both the conductive and convective behavior of the structure, resulting in a significant impact on the sensitivity of manufactured devices.

Based on an existing behavioral model, we have established new physically-based expressions for the heater thermal resistance (which drives the actual heater temperature for a given biasing voltage) and for the common mode temperature of detectors. A semi-empirical expression has also been established for the differential temperature of detectors. All these expressions involve not only the lateral dimensions of the sensors but also the cavity depth h_1, the latter being the more likely parametric fault in an industrial process. A very good agreement has been found between this behavioral model and FEM simulations.

Finally, the proposed model allows the realistic simulation of a convective accelerometer with a single electrical input, i.e. the biasing voltage of the heater beam. It allows evaluating process scatterings using behavioral models as Monte-Carlo simulations are achievable in a reasonable CPU time compared to FEM simulations. It is therefore very useful to explore potential correlations between different parameters. In particular, we have established that a correlation between the common mode temperature of the detectors and the differential temperature of the detectors exists.

Future work involves further exploration of such correlations in order to define alternate test procedures able to verify and/or estimate sensor sensitivity. Another perspective concerns the refinement of the model in order to include the influence of the package on the behavior of the final product.

REFERENCES

[1] B. Charlot, S. Mir, F. Parrain, B. Courtois, "Generation of electrically induced stimuli for MEMS self-test", Journal of Electronic Testing - Theory and Applications (JETTA), Vol.17, No. 6, December 2001.

[2] N. Dumas, F. Azaïs, F. Mailly, P. Nouet, *Evaluation of a fully electrical test and calibration method for MEMS capacitive accelerometers*, Proc. IEEE Int'l Mixed-Signals, Sensors and Systems Test Workshop (IMSTW'08), Vancouver, Canada, 18-20 June 2008.

[3] V. Natarajan, S. Bhattacharya, A. Chatterjee, *Alternate Electrical Tests for Extracting Mechanical parameters of MEMS Accelerometer Sensors*, Proc. IEEE VLSI Test Symposium (VTS'06), April30 -May4 , 2006.

[4] M.G. da Silva, G. Schröpfer, B. Blackwell and A. Ramalingam, *Designing MEMS for Reliability (DFR)*, International Conference On Emerging Research And Advances In Mechanical Engineering, 16-18 February 2007.

[5] X.B. Luo, Z.X. Li, Z.Y. Guo and Y.J. Yang, *Study on linearity of a micromachined convective accelerometer,* Microelectronic Engineering 65 (2003) 87-101.

[6] A. Chaehoi, F. Mailly, L. Latorre and P. Nouet, *Experimental and finite-element study of convective accelerometer on CMOS*, Sens. Actuators A 132/1 (2006), p. 78-84.

[7] A.A. Rekik, F. Azais, N. Dumas, F. Mailly, P. Nouet, M. Masmoudi, *Investigations on Electrical-only Test Setup for MEMS Convective Accelerometer*, 3rd IEEE International Conference on Signals, Circuits and Systems (SCS 2009), Djerba, Tunisia, 5-8 November 2009.

[8] A.A. Rekik, F. Azaïs, N. Dumas, M. Masmoudi, F. Mailly, P. Nouet, *A study of package effects on the behavior of MEMS convective accelerometers*, Design, Test, Integration and Packaging of MEMS and MOEMS (DTIP 2010), Seville, Spain, 5-7 May 2010.

[9] O. Leman, A Chaehoi, F. Mailly, L. Latorre, P. Nouet, "*Modeling and system-level simulation of a CMOS convective accelerometer*", Solid-State Electronics, Volume 51, Issues 11-12, pp. 1609-1617, 2007.

[10] O. Leman, F. Mailly, L. Latorre and P. Nouet, *HDL Modeling of convective accelerometers for system design and optimization*, Sens. Actuators A 142 (2008), p. 178-184.